Numerical modelling of medical ultrasound: reconstruction of wavefront after an aberrator

Katerina A. Beklemysheva[1], Georgiy K. Grigoriev[3], Nikolay S. Kulberg[4,5], Igor B. Petrov[1], Aleksey V. Vasyukov[1], Yuri V. Vassilevski[1,2]

[1]MIPT, 9 Institutskiy per., Dolgoprudny, Moscow Region, 141700
[2]INM RAS 8 Gubkina str., Moscow, 119333
[3]MGTS Medical and health center, Petrovsky blvd., 12, bld. 1, Moscow, 127051
[4]Moscow Scientific and Practical Center of Medical Radiology, Srednaya Kalitnikovskaya street, 28, bld. 1, Moscow, 109029
[5]IEI FRC CSC RAS 44, block 2, Vavilov Str., Moscow 119333
E-mail: yuri.vassilevski@gmail.com

Abstract

Modelling of transcranial ultrasound requires to consider the bone layer which acts as an ultrasound aberrator – a complex shape object with different ultrasound wave speed. In this article, the scanning of medical phantom was performed through silicon aberrators with wave notching. For the reconstruction of ultrasound wave front after the aberrator a wavefront construction raytracing method for two dimensional acoustics is implemented. B-scans are obtained and compared with experimental data.

Keywords: medical ultrasound, raytracing, wavefront construction raytracing, model verification

MSC 2010: 65M25

Received: ???

The work on numerical modelling of ultrasound scanning of biological objects was started by the authors in [1] and [2]. It concentrated on developing and veryfying a modelling technique for ultrasound propagation in complex areas, including contacts between tissues with significantly different mechanical properties and with complicated contact surfaces. In the current paper, we implemented another numerical method to improve performance.

Grid-characteristic method (GCM), used in the previous work, can manage any kind of border and contact conditions, allowing to analyze complex stress patterns in high spatial definition. In case of transcranial ultrasound, the required spatial definition for the whole transcranial area leads to an enormous calculation time. Another problem is that a wavefront has a finite size. When modelling a complex multilayered medium with GCM, wavefronts merge with each other. It is necessary to consider the wavefront size in case of a possible destruction caused by elastic waves interference – a crack or a break-off. In diagnostic ultrasound the wave amplitude is too low to cause damage. At the same time, the waves merging complicates the analysis of the wave pattern. The raytracing method allows to isolate any wavefront and analyze its path from its generation to the complete fading. GCM will be used to obtain solutions for certain statements that are hard to solve analytically – for example, critical angles on a contact of elastic materials or material behavior on sharp edges.

A raytracing method that we suggest to use for the problem of transcranial ultrasound needs an introduction.

1 Introduction

The majority of research on the medical ultrasound uses the acoustic material model ([3]) that doesn't consider shear waves. This assumption works well for soft tissues and MHz frequencies that are used in diagnostic ultrasound ([4]). Shear waves leave their trace on the signal obtained from the area directly beneath the sensor, increasing the blind area of the device, but they fade too quickly to reach anything else.

The final goal of this work is to develop a numerical method for the transcranial ultrasound which requires to consider the bone layer that can't be modeled without shear and surface waves. Most part of longitudinal waves that fall on the contact between elastic bodies generate shear waves and vice versa ([5]). In bones, shear waves fade much slower and travel much faster than in soft tissues. In case of a transcranial area it can noise the resulting picture – a shear wave can go around the skull, generate a longitudinal wave and leave a signal on

the sensor before the ultrasound response from a brain vessel reaches it. The same applies to surface waves.

Similar problems are quite typical for a different science field – seismic exploration. A lot of research in this area was also limited by acoustic model ([6]), but modern seismics is mostly devoted to elastic materials, including anisotropic ones. One of the most popular and detailed book about seismic mechanics is [5] – various ways of signal generation, reverse problems, data analysis and seismometry. The authors give analytic relations of the amplitudes of the secondary waves upon reflection from the free boundary and refraction at the contact between two elastic media for the simplest geometries – the plane boundary, plane and spherical fronts, plain layers, etc. Surface waves are also considered, but the authors do not provide a sufficiently detailed analytics for their connection with critical angles, which makes it difficult to directly apply their formulas for practical calculations.

Consideration of surface waves generated by a reflection in the medium is not so relevant for seismic exploration. The Rayleigh waves that appear in a surface explosion that triggers a diagnostic pulse into the Earth's depth can leave a signal on the sensor and drown out the response from the area near the surface. The Rayleigh and Lamb waves, which appear in an earthquake (more precisely, when a longitudinal wave is reflected from the surface and re-reflected in geological layers), carry energy over a long distance and cause destruction. In each of these cases, to analyze the effect of surface waves, it is sufficient to consider the wave that has already formed, without analyzing in detail the mechanics of its generation.

Surface waves that are generated deep inside the medium do not affect the signal on the seismic sensors, since they propagate more slowly than shear waves and either diverge from the receivers or do not give sufficiently strong reflections due to poor interaction with other media. In this situation, we should take into account the characteristic geometry of the problem – seismics is characterized by a layered area with almost horizontal boundaries, where inclusions of any complex form are relatively small (caverns and cracks with air, water or oil).

Modeling of transcranial ultrasound by GCM [1] makes it possible to obtain these waves without delving into the physics of their generation. When a complete system of equations for an elastic medium is solved at each grid node (including interfaces and contacts), these waves are taken into account automatically. With the transition to the raytracing method, it is possible to obtain a significant increase in performance and simplify the analysis of the wave pattern, since even with interference we can isolate specific interacting fronts. However, in this case it is necessary to directly simulate all wave processes,

including surface waves.

The raytracing method ([7]) is used in many fields: computer graphics ([8]), radiolocation, underwater acoustic location, medical and industrial ultrasound, optics and seismics ([9], [11]). Each field has its specifics, which changes the priorities in the method development.

In the paper [10] kinematic relations for elastic waves and formulas for amplitudes in inhomogeneous anisotropic media are derived.When considering the direct problem of modeling the propagation of waves from a source to a receiver for given medium parameters, the eikonal equation is solved, which allows obtaining the arrival time of the waves on the receiver and their amplitudes [12], [13].

The network ray tracing method or the shortest ray path method was developed to overcome the limitations of the conventional ray tracing method, such as the paths of diffracted beams and paths to shadow zones, using the shortest or fastest path through a network of speed-separated blocks [14]. This method is also called the graph method, since the shortest path is calculated on the graph in which the vertices are the nodes of the geometric grid. In the case of complex geometry, such a graph grows rapidly, and the calculation becomes extremely long [15]

The wavefront construction method (WFC) expands the conventional raytracing method [16], [17], [18]. In this variation of the method, instead of individual independent rays, wave fronts are modeled – in the three-dimensional case they are surfaces whose fineness can be dynamically varied, adding new rays by interpolating neighboring ones. This helps to avoids artificial shadows, which in the original method could appear with insufficient number of rays. For medical ultrasound, it helps to model point reflectors – objects that are too small to be effectively detected by a basic raytracing implementation. This method is also implemented for anisotropic media [19]. Features of front grid generation are considered in [11].

The WFO (WaveFront Oriented) method, similar to the previous one, instead of interpolating recalculates a new ray from the source [20]. This slightly reduces performance, but increases the fineness of the front.

A comparison of the listed implementations was done in [21]. The graph method was the longest, and the FDES method (finite-difference eikonal solver, the method of solving the eikonal equation based on the finite difference method [22]) produced the greatest errors.

The propagation of surface waves is considered, for example, in [24], [5] and [23]. We were unable to find articles devoted to modeling of surface waves by ray tracing method or detailed analytics on their

generation with regard to critical angles.

In this paper, we implemented a two-dimensional wavefront construction method for acoustic material model. It can process point reflectors and explicit contact surfaces of a complex form, considering reflection, refraction and attenuation. This method is not as good for parallelization as the traditional raytracing method, but it was chosen for its capacity for dynamic mesh refinement and point reflectors processing.

The structure of this paper is as follows. In Section 2 we present governing equations for wave propagation problems and the description of the method. Section 3 describes experimental setup – a phantom and aberrators used and scanning signal properties. In Section 4 several model statements are presented to illustrate the behavior of wavefronts in the presence of an aberrator. Section 5 contains the comparison of experimental and calculation data. Section 6 contains the concusion.

2 Ultrasound propagation model

2.1 Governing equations and discretization

The modelling is based on acoustic model [2]. Ultrasound propagation is described with the following equation:

$$\rho(\mathbf{x})\frac{\partial \mathbf{v}(\mathbf{x},t)}{\partial t} + \nabla p(\mathbf{x},t) = 0 \qquad \text{in } \Omega, \quad (2.1)$$

$$\frac{\partial p(\mathbf{x},t)}{\partial t} + \rho(\mathbf{x})c^2(\mathbf{x})\nabla \cdot \mathbf{v}(\mathbf{x},t) = -\alpha(\mathbf{x})c(\mathbf{x})p(\mathbf{x},t) \qquad \text{in } \Omega,$$

where Ω is the domain occupied by the tissues, $\mathbf{x}$ is a point in Ω, $\rho(\mathbf{x})$ is the density, $\mathbf{v}(\mathbf{x},t)$ is the velocity vector, $p(\mathbf{x},t)$ is the acoustic pressure, $c(\mathbf{x})$ is the speed of sound, $\alpha(\mathbf{x})$ is the attenuation coefficient according to the Maxwell model [2].

The model takes into account longitudinal (pressure) waves in tissues and does not describe transverse (shear) waves. This approach is used since attenuation coefficient for shear waves is four orders of magnitude greater than that for pressure waves at MHz frequencies [4].

2.2 Wavefront construction raytracing

The application of raytracing method to medical problems is complicated by artificial shadows. If a complex shaped aberrator distorts the wavefront, angle and distance between adjacent rays may become

larger. In the basic raytracing method rays are calculated independently and we do not have means to correct or even trace that situation during the calculation. In case of simple geometry (for example, several thick and wide layers or a single cylinder in a homogenous medium), the amount of rays can be estimated before the calculation. Calculation grids based on the real anatomy of a human body are too intricate for such an analysis. Even medical phantoms has objects that are hard to resolve by a conventional raytracing – point reflectors, usually implemented as thin nylon threads (about 0.1 mm thickness against the 10-20 cm of the characteristic size of a phantom). Resolving them head-on requires a number of rays that makes the raytracing method too slow to be effective in comparison with grid methods.

The wavefront construction method (WFC) expands the conventional raytracing method [16], [17], [18]. The main idea behind this method is a local dynamic tuning of the amount of rays on every time step by keeping neighbors of every ray and checking the distance to them. It, obviously, helps to maintain the density of the ray field, but also can easily consider the point reflectors.

In a three-dimensional space, wavefronts are surfaces that can be approximated as triangular grids. This is a separate problem, and it is considered in [11]. For the modelling of a medical phantom and for the testing of applicability of the method to the aberrator problem the two-dimensional approach is enough. Because of the simple structure of the medical phantom under consideration, objects outside the focused ultrasound ray don't influence the signal on the sensor. In 2D case, wavefronts become curves that can be approximated as chains of segments.

In this article, we based on the approach from [16], where the detailed mathematics for the WFC method is given, with several modifications. The first small difference is that we used a linear approximation for the new rays instead of a cubic one. The second small difference is the addition of point reflectors – when a wavefront segment crosses a point reflector, it emits a reflected semicircumference wave. The main difference is that we implemented explicitly defined interfaces between different materials according to the Snell's law [5]. That step was necessary before the transition to 3D, because the wavefront reconstruction after the reflection and refraction has a lot of technical complexities even in 2D.

The following is a description of the algorithm for interface calculation. In case of acoustics (unlike elasticity) a ray, falling on a contact between two materials (ray A), generates two rays – a reflected ray (ray B, heading back to the same material) and a refracted ray (ray C, heading towards the second material). For each of the two new rays,

we calculate amplitudes according to the Snell's law and we must appoint neighbors. A simple copying of neighbors from ray A will lead to the bifurcation of the wavefront, complicating the wave pattern analysis. Also, another problem arises with wavefront grid refinement between different materials.

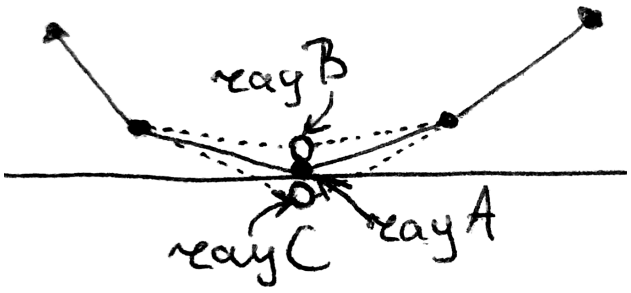

Figure 1: Virtual nodes for a simple reflection and refraction

To avoid these problems, we used a system of virtual neighbors. Neighbors of ray A become mutual virtual neighbors with rays B and C. A general scheme is given on Fig. 1, where points designate current ray positions and segments designate real neighbors. In calculation, rays B and C have the same position as the ray A – on the scheme they are displayed with a shift to illustrate the algorithm.

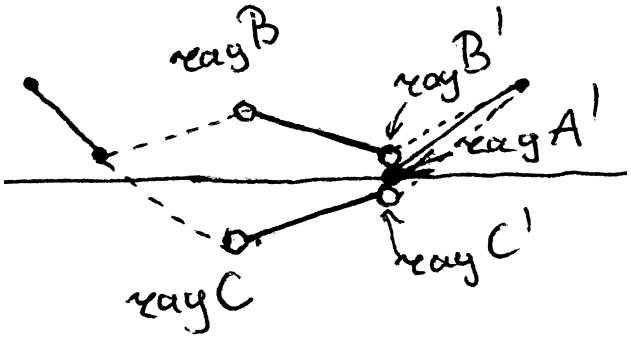

Figure 2: Reconstruction of wavefront after reflection and refraction

This applies to the situation when ray A have only real nodes. The situation when the falling ray has virtual neighbors is presented on Fig. 2. Ray A was deleted after the previous step and replaced

with rays B and C. All rays were moved according to their velocities. The falling ray is designated as A', reflected and refracted – as B' and C' accordingly. The right neighbor of ray A' becomes a virtual right neighbor for rays B' and C'. Left virtual neighbors of ray A' become real neighbors for rays B' and C', according to the material they are in. Thus, both wavefronts are restored, the reflected one and the refracted one.

The elementary calculations, illustrating the restoration of wavefronts, are given on Fig. 3. A point explosion in a medium consisting of a homogeneous background and an extended inclusion – a layer – with differing rheological properties is considered.

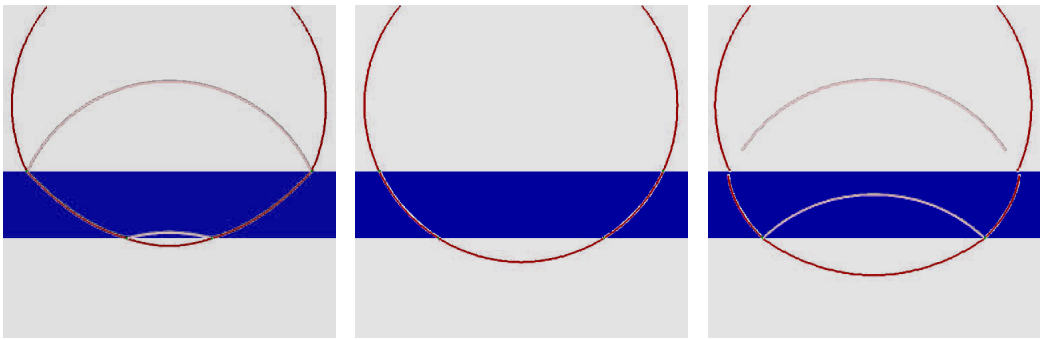

a) b) c)

Figure 3: Wave pattern after the obstacle: a – obstacle relative sound speed 0.8, b – obstacle relative sound speed 1.0, c – obstacle relative sound speed 1.2

The figure shows that the calculation is qualititavely correct:

- the spherical wave front after passing through the boundary is restored correctly – without rips or "extra" edges;
- the front of a head wave in a material with a lower sound velocity has the expected shape of a "bow" ([5]);
- the reflection is weaker when the material properties are slightly different;
- after passing through the obstacle, the shape of the wavefront is restored.

The attenuation is also considered, both scattering in space and Maxwell's fading in a material. Rays that are too weak to leave a signal on the sensor are instanteously dropped from the calculation.

3 Problem statement and experiment setup

The ultrasound phantom ??? was considered. We modelled only multiple point reflectors with brightness 5%. In this phantom, there are no tubes with water, and modeling of gray background at this stage is difficult in terms of calculation time.

The aberrator is flat on one side and has a wavy surface on the other. Two aberrators were considered - with five waves and with three waves. The casting mold was printed on a 3D printer, the general form of the mold for the five-wave aberrator is presented on Fig. 4).

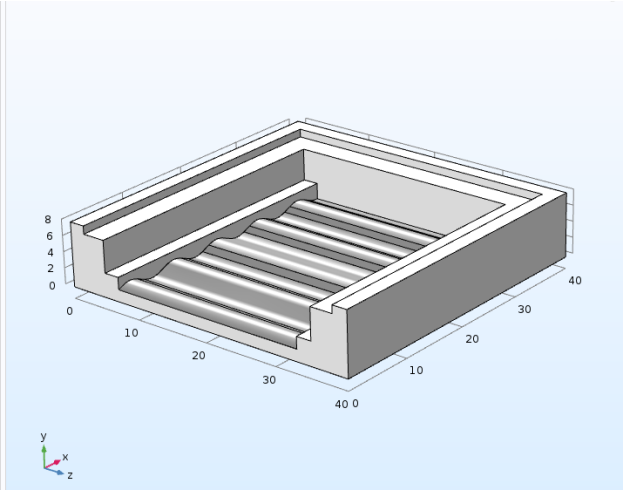

Figure 4: General view of the casting mold for the silicon aberrator with five waves

3.1 Ultrasound scanner

Ultrasound scanner with a linear phased array of 48 elements was used for this research. Operational frequencies vary from 2 MHz to 7.5 MHz. The transmitted signal for the measurements had base frequency $\Omega = 3$ MHz and $\sigma = 1$ MHz. So, according with three-sigma rule of thumb, practically meaningful part of the spectrum is from 0 to 6 MHz. Based on this fact, experimental data is digitized using 12 MHz frequency. Numerical modelling also obtains samples using this frequency to allow direct comparation between experimental and modelling results. Each ray falling on an element leaves a single signal on it.

The details about signal processing and B-scan generation are given is out previous article [2].

4 Model statements

Since the wave pattern in the experimental statement is too complex for the article format, we used several simple statements to illustrate the influence of a wave-notched aberrator on a wavefront from a point reflector.

Fig. 5 and 6 show the dynamic wave pattern for the three wave notched aberrator and a single point reflector. The position of the reflector was chosen so its signal will come to the sensor later than the signal from aberrator boundaries. Fig. 7 and 8 show the dynamic wave pattern for the five wave notched aberrator. For every statement, a reference calculation without an aberrator is given – if the material of the aberrator is the same with the background material, it does not influience the wave pattern.

Multiple reflections in aberrator complicate the wave pattern. Each curve of the aberrator notching reflects a distinct wave, which overlap and generate even more reflections after the next encounter with the notched surface. If we modeled the same statement with a grid method, these wavefronts would have merged into a single wide weak wavefront. Raytracing highlights every single wavefront, allowing us to backtrace any of them.

The initial pulse is strong, and generates several reflections, the exact amount depends on the attenuation parameter and the sound speed difference. The wave from the point reflector is much weaker, and its reflections from the aberrator do not appear.

The spherical wavefront after the aberrator has a characteristic wave-shaped distortion. The focusing algorithm for B-scan generation interprets a circumference wavefront as a point in the center of this circumference. If this point is deviated from the focusing direction or too far from the focusing distance, it will be blurry. But if we adjust the position of the sensor, the aberrator will give several shadows of the point reflector, each wave giving a shadow. The closer a point reflector to the aberrator and sensor, the smaller is the distance between shadows.

B-scans, presented on Fig. 9 and 10, show that the point reflector signal can be easily lost in the signal fron aberrator boundaries. If the notched side of the aberrator is in the sensor direction, we can see distinct bright points that are causes by reflections from notches.

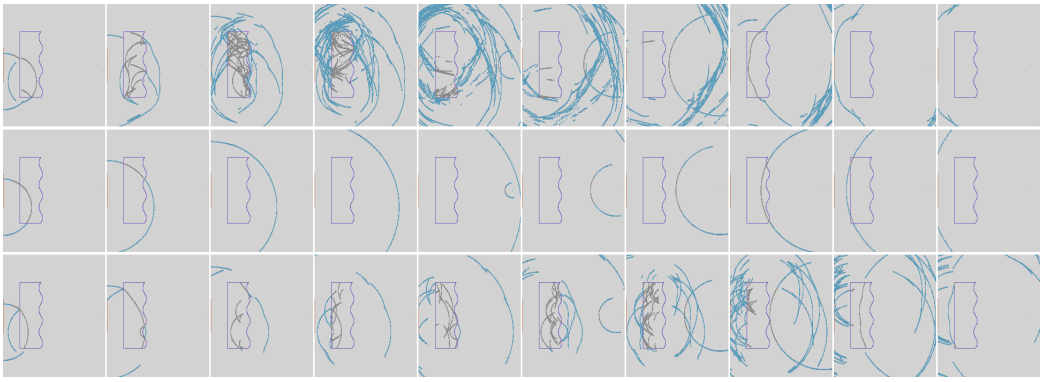

Figure 5: The passage of a spherical wavefront and its reflection from a single point reflector through a three wave notched aberrator obstacle, notching at the phantom side. From left to right – consequent time steps. From top to bottom – relative sound speed of the aberrator is 0.7, 1.0, 1.43 accordingly

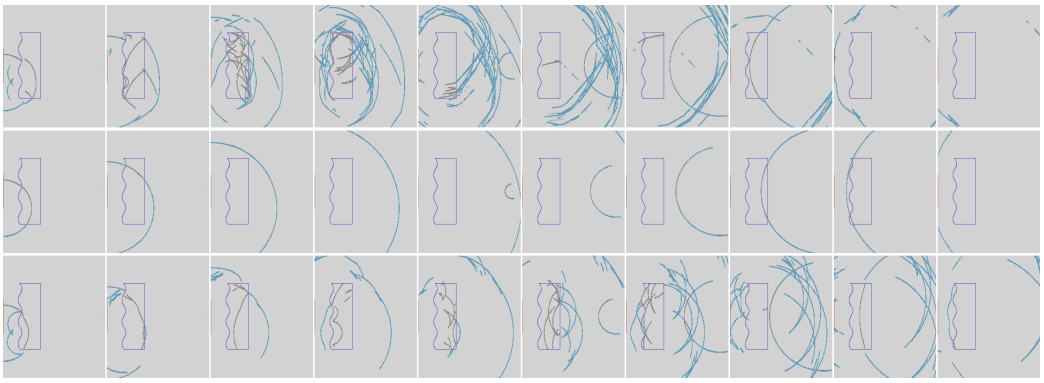

Figure 6: The passage of a spherical wavefront and its reflection from a single point reflector through a three wave notched aberrator obstacle, notching at the sensor side. From left to right – consequent time steps. From top to bottom – relative sound speed of the aberrator is 0.7, 1.0, 1.43 accordingly

5 Comparison of numerical and experimental data

The comparison of experimental and calculated B-scans is given on Fig. 11. Without an aberrator, calculated B-scan generally corresponds to the experiment.

The five waves aberrator that was used multiplies the vertical line of points and the dense group of points. Only three shadows are visible. Model statements show that it happens because of a comparative

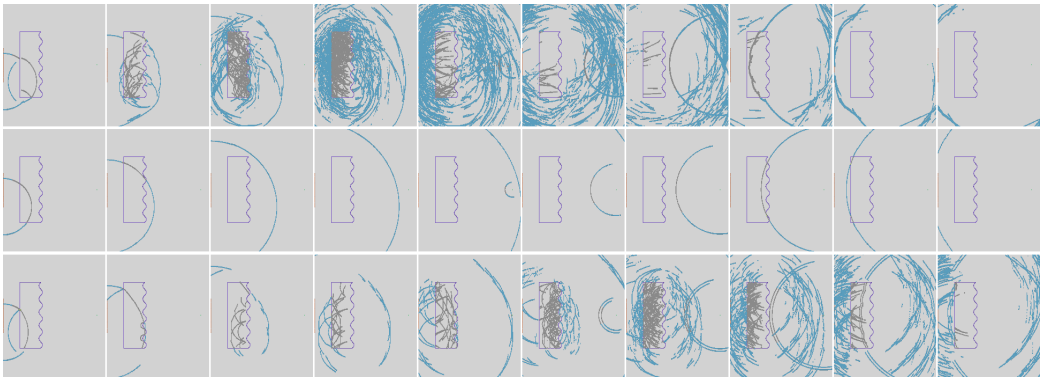

Figure 7: The passage of a spherical wavefront and its reflection from a single point reflector through a five wave notched aberrator obstacle, notching at the phantom side. From left to right – consequent time steps. From top to bottom – relative sound speed of the aberrator is 0.7, 1.0, 1.43 accordingly

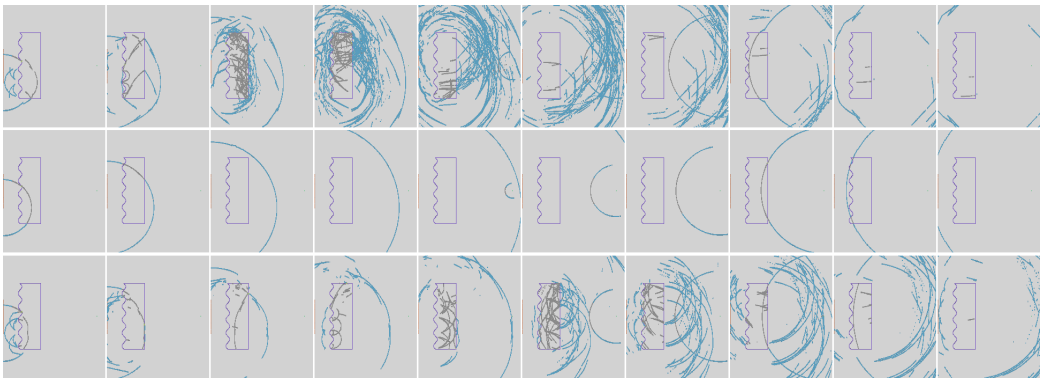

Figure 8: The passage of a spherical wavefront and its reflection from a single point reflector through a five wave notched aberrator obstacle, notching at the sensor side. From left to right – consequent time steps. From top to bottom – relative sound speed of the aberrator is 0.7, 1.0, 1.43 accordingly

size of sensor and aberrator – only three circumferences, caused by aberrator distortion, get to the sensor.

6 Conclusions

The final goal of this long-term work is to develop a methodology for the modelling of the transcranial ultrasound, which includes a material model, a numerical method and an analysis of the mechanisms involved in this process.

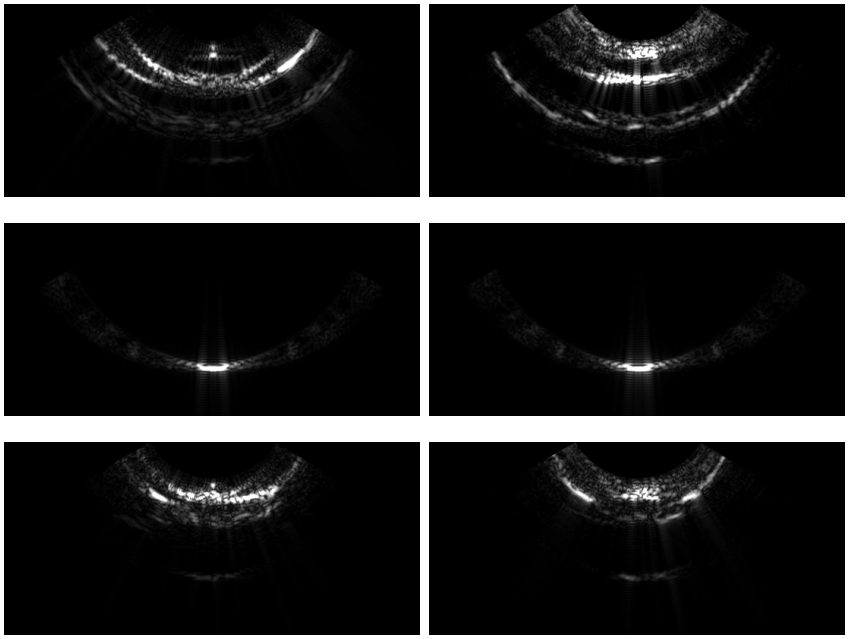

Figure 9: B-scans for the three-wave notched aberrator and the single point reflector. On the left – notching at the phantom side, on the right – notching at the sensor side. From top to bottom – relative sound speed of the aberrator is 0.7, 1.0, 1.43 accordingly

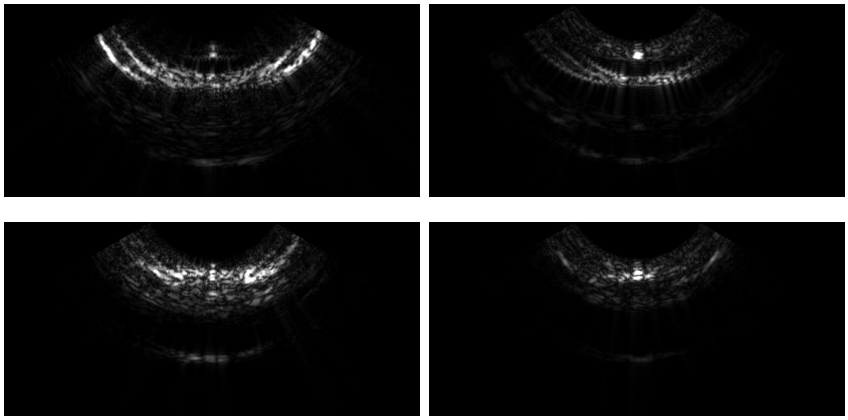

Figure 10: B-scans for the five-wave notched aberrator and the single point reflector. On the left – notching at the phantom side, on the right – notching at the sensor side. From top to bottom – relative sound speed of the aberrator is 0.7 and 1.43 accordingly

In this article, we implemented the wavefront construction numerical method for two dimensional acoustics to model the scanning of

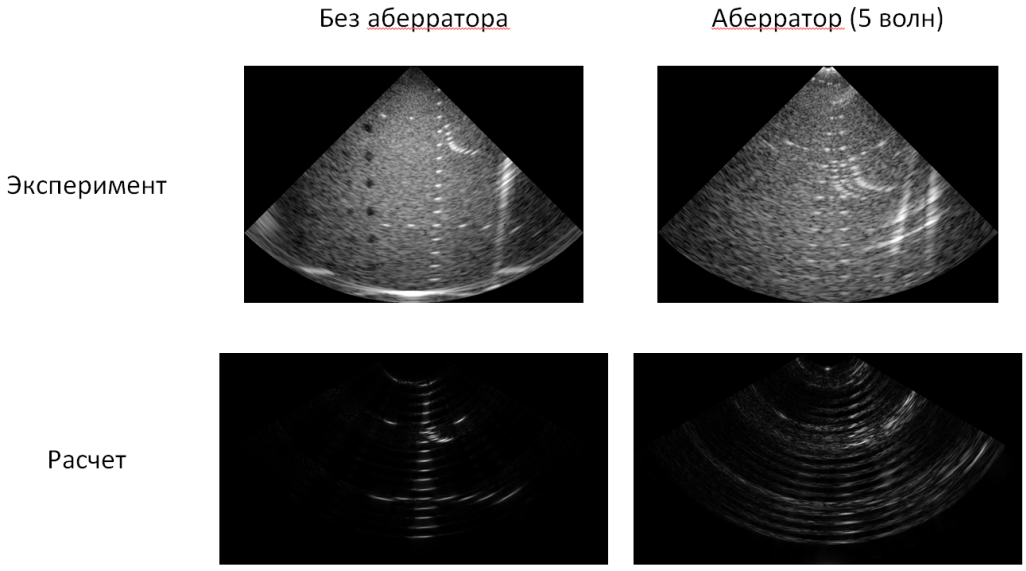

Figure 11: Experimental and calculated B-scans

medical phantom through silicon aberrators with wave notching. Explicitly defined interfaces were introducted, where wavefront reconstruction was performed using virtual neighbors. Obtained B-scans showed a good agreement with experimental data for point reflectors. Wave patterns for model statements allow to analyze the process of wavefronts interaction with the aberrator, explaining the nature of aberrations on B-scans.

The wavefront construction method showed good results for the medical phantom. For its application to the transcranial ultrasound problem, several modifications must be made. Primarily, the elastic material model must be implemented, including the contact between elastic and acoustic materials. Secondly, the 3D implementation is required to model the complex geometry of a human craniocerebral area.

Funding: The research was supported by RSF grant 14-31-00024.

References

[1] K. A. Beklemysheva, A. A. Danilov, G. K. Grigoriev, A. O. Kazakov, N. S. Kulberg, I. B. Petrov, V. Yu. Salamatova, Yu. V. Vassilevski, A. V. Vasyukov, Numerical modelling of medical ultrasound: phantom-based verification. *Russian Journal of Nu-*

merical Analysis and Mathematical Modelling, (2016) **31**, No. 5, 317-328

[2] K. A. Beklemysheva, G. K. Grigoriev, N. S. Kulberg, I. B. Petrov, Yu. V. Vassilevski, A. V. Vasyukov, Transcranial ultrasound of cerebral vessels in silico: proof of concept. *Russian Journal of Numerical Analysis and Mathematical Modelling*, (2017) **?**, No. ?, 1-11

[3] N. M. Tole H. Ostensen, Basic Physics of Ultrasonographic Imaging. *World Health Organization*, (2005)

[4] E. L. Madsen, H. J. Sathoff, and J. A. Zagzebski, Ultrasonic shear wave properties of soft tissues and tissuelike materials. *J. Acoust. Soc. Am.* (1983) **74**, No. 5, 1346-1355.

[5] K. Aki, P. Richards, Quantitative seismology. Theory and methods *W.H. Freeman and Company, San Francisco*, (1980)

[6] .., : . . .-. .

[7] G. H. Spencer M. V. R.K. Murty, General ray tracing Procedure. *J. Opt. Soc. Am.*, (1962) **52**, No. 6, 672-678

[8] I. Wald W.R. Mark J. Gunther S. Boulos T. Ize W. Hunt S.G. Parker P. Shirley, State of the art in ray tracing animated scenes. *Eurographics 2007 State of the Art Reports*, (2007) 89-116

[9] erven V., Seismic ray theory. *Cambridge University Press, New York*, (2001)

[10] erven V., Seismic Rays and Ray Intensities in Inhomogeneous Anisotropic Media. *Geophys. J. R. astr. Soc.*, (1972) **29** 1-13

[11] K.J. Lee, Efficient ray tracing algorithms mased on wavefront construction and model bades interpolation method, PhD dissertation. *M.S., Texas A&M University*, (2005)

[12] Qian J. Symes W., An adaptive finite-difference method for traveltimes and amplitudes. *Geophysics*, (2002) **67** 167-176

[13] Buske S. Kastner U., Efficient and accurate computation of seismic traveltimes and amplitudes. *Geophys. Prosp.*, (2004) **52** 313-322

[14] Moser T. J., Shortest path calculation of seismic rays. *Geophysics*, (1991) **56** 59-67

[15] van Avendonk H. J. A. Harding A. J. Orcutt J. A. Holbrook W. S., Hybrid shortest path and ray bending method for traveltime and raypath calculation. *Geophysics*, (2001) **66** 648-653

[16] Vinje V. Iversen E. Gjystdal H., Traveltime and amplitude estimation using wavefront construction. *Geophysics*, (1993) **58** 1157-1166

[17] Lambare G. Lucio P. S. Hanyga A., Two-dimensional multivalued traveltime and amplitude maps by uniform sampling of a ray field. *Geophys. J. Int.*, (1996) **125** 584-598

[18] Lucio P. S. Lambare G. Hanyga A., 3D multidimensional travel time and amplitude maps. *Pure Appl. Geophys.*, (1996) **148** 449-479

[19] Gibson, R. L. Jr., Ray tracing by wavefront construction in 3-D, anisotropic media. *Amer. Geophys. Union*, (1999) **80**

[20] Coman R. Gajewski D., Ray tracing by wavefront construction in 3-D, anisotropic media. *71st Internat. Meeting Abstract, Soc. Expl. Geophys.*, (2001) 1265-1268

[21] Leidenfrost A. Ettrich N. Gajewski D. Kosloff D., Comparison of six different methods for calculating traveltimes. *Geophys. Prosp.*, (1999) **47** 269-297

[22] Kim S. Cook R., 3-d traveltime computation using second-order eno scheme. *Geophysics*, (1999) **64** 1867-1876

[23] Crampin S., The dispersion of surface waves in multilayered anisotropic media. *Geophys. J. R. astr. Soc.*, (1970) **21** 387-402

[24] Lord Rayleigh, On Waves Propagated along the Plane Surface of an Elastic Solid. *Proc. London Math. Soc.*, (1885) **1** 4-11